Bond-space operator disentangles quasilocalized and phononic modes in structural glasses

Julia A. Giannini,[1,2,*] David Richard,[1,3] M. Lisa Manning,[1,2] and Edan Lerner[3,†]
[1]*Department of Physics, Syracuse University, Syracuse, New York 13244, USA*
[2]*BioInspired Institute, Syracuse University, Syracuse, New York 13244, USA*
[3]*Institute for Theoretical Physics, University of Amsterdam, Science Park 904, Amsterdam, Netherlands*

(Received 11 August 2021; accepted 20 September 2021; published 13 October 2021)

The origin of several emergent mechanical and dynamical properties of structural glasses is often attributed to populations of localized structural instabilities, coined *quasilocalized modes* (QLMs). Under a restricted set of circumstances, glassy QLMs can be revealed by analyzing computer glasses' vibrational spectra in the harmonic approximation. However, this analysis has limitations due to system-size effects and hybridization processes with low-energy phononic excitations (plane waves) that are omnipresent in elastic solids. Here we overcome these limitations by exploring the spectrum of a linear operator defined on the space of particle interactions (bonds) in a disordered material. We find that this bond-force-response operator offers a different interpretation of QLMs in glasses and cleanly recovers some of their important statistical and structural features. The analysis presented here reveals the dependence of the number density (per frequency) and spatial extent of QLMs on material preparation protocol (annealing). Finally, we discuss future research directions and possible extensions of this work.

DOI: 10.1103/PhysRevE.104.044905

I. INTRODUCTION

Glasses and other amorphous solids represent a class of materials that is both relatively commonplace and highly complex. Traditional glasses can be engineered to have desired mechanical and optical properties and have been used in commercial and technological applications for decades [1–3]. Despite their familiarity, the fundamental physics underlying several common features of glasses is not yet well understood. For example, thermodynamic and mechanical properties of disordered solids, such as the dependence of heat capacity on temperature [4] and material response to external deformation [5,6], vary nontrivially from those of crystalline solids.

While amorphous materials respond elastically to small applied strain, they undergo irreversible structural rearrangement for moderate deformation that is difficult to characterize and predict [3]. In early studies of metallic glasses, researchers identified localized regions of stress-induced plastic deformation that are responsible for yielding behaviors such as shear banding and avalanches [7]. Falk and Langer analyzed micromechanical features that give rise to localized irreversible rearrangements in simulated solids and termed such glassy defects shear transformation zones (STZs) [8]. Recently, significant effort has been put into forming structure-dynamics predictions for the failure behavior of disordered solids [1,3,9–14]. These works attempt to identify structural precursors to plastic deformation, which occurs when glasses become unstable.

Many methods for detecting STZs in glasses build upon Goldstein's potential energy landscape (PEL) picture [3,13,15–17]; for a disordered solid in d spatial dimensions with a total potential energy U that depends on Nd degrees of freedom, the PEL is a Nd-dimensional surface that governs the system's mechanics. It is commonly accepted that the intrinsic structural-mechanical disorder of glasses is manifested in the complexity or "ruggedness" of the PEL, which features a multiplicity of local minima that is exponential in the number of particles N. Mechanically stable configurations sit in local minima of the PEL, and applied deformation, forcing, or thermal activity can push the system into adjacent minima, constituting irreversible particle rearrangements. In the framework of linear response theory, one analyzes local curvatures of the PEL by computing the Hessian matrix $\mathcal{M} \equiv \frac{\partial^2 U}{\partial \vec{X} \partial \vec{X}}$, where $\vec{X}$ denotes particle coordinates. Diagonalization of $\mathcal{M}$ gives access to a glass's vibrational modes $\vec{\psi}_l$, with associated vibrational frequencies ω_l, satisfying $\mathcal{M} \cdot \vec{\psi}_l = \omega_l^2 \vec{\psi}_l$ (setting all masses to unity). Under a restricted set of conditions [18–20], low-frequency harmonic modes can cleanly localize on small groups of particles and constitute good representations of STZs in glasses [3,21]. These soft quasilocalized modes (QLMs) are key candidates for two-level systems whose presence can explain the thermodynamic and mechanical anomalies of glassy behavior [4].

QLMs are soft excitations that emanate from the structural disorder and mechanical frustration of glasses. A subset of these excitations constitute glasses' carriers of plastic deformation [21]. It is now well established that the density $D(\omega)$ of QLMs—per frequency and per particle—follows a universal form, scaling as ω^4, independent of spatial dimension [22], glass preparation protocol [23,24], or microscopic-interaction

*jagianni@syr.edu
†e.lerner@uva.nl

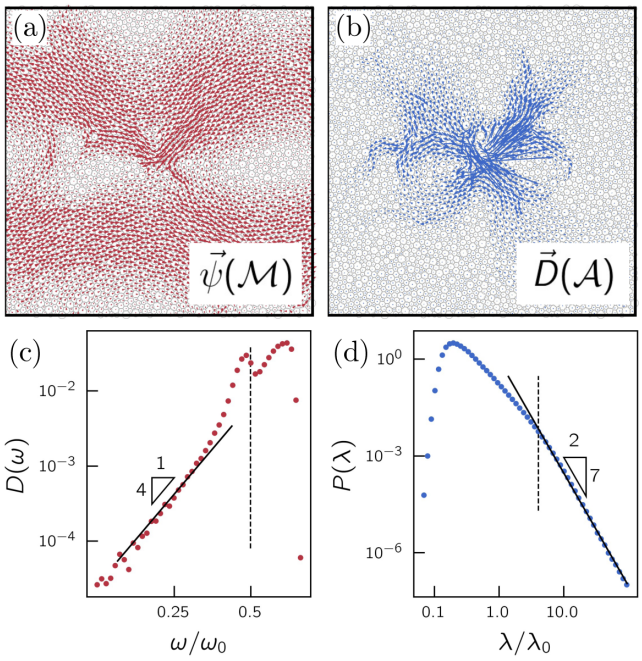

FIG. 1. A single soft mode in a two-dimensional (2D) computer glass with $N=4096$ as revealed by (a) the Hessian matrix $\mathcal{M}$ and by (b) the bond-force-response operator $\mathcal{A}$, see text for details. The clear phonon hybridization of the Hessian mode of panel (a) is entirely suppressed in the corresponding $\mathcal{A}$ mode of panel (b), cleanly revealing a *quasilocalized mode*. (c) Harmonic spectrum $D(\omega)$ vs frequency ω for computer glasses in three dimensions (3D), featuring the universal asymptotic $\sim\omega^4$ scaling. The vertical line marks the expected lowest phonon frequency $\omega_{\rm ph}=2\pi c_s/L$ with c_s denoting the shear wave speed and L denoting the linear size of the glass. All frequencies are divided by $\omega_0=c_s/a_0$, where $a_0\sim\rho^{-1/d}$ and ρ is the density of the system (with particle masses set to unity). (d) Distribution of eigenvalues $P(\lambda)$ of $\mathcal{A}$ calculated for the same glasses as (c). All eigenvalues are divided by $\lambda_0=\omega_0^{-2}$ for sake of comparison with the spectrum of the Hessian. The observed $P(\lambda)\sim\lambda^{-7/2}$ scaling at large λ echoes the $\sim\omega^4$ scaling of the nonphononic spectrum of (c), as we explain in what follows. The vertical line marks the λ value corresponding to the expected lowest phonon frequency in the system, $\lambda_{\rm ph}\sim\omega_{\rm ph}^{-2}$

details [25]. However, (linear) continuum elasticity dictates that the vibrational spectrum of a solid must include long-wavelength phononic excitations. Since QLMs and phonons are not necessarily orthogonal, hybridization processes between the two—as visualized in Fig. 1(a)—obscure the important information contained in QLMs [19,26].

To overcome the aforementioned phonon hybridization effects on QLMs, novel techniques and computational frameworks have been developed. These include a family of nonlinear excitations [13,21,26,27], termed nonlinear plastic modes (NPMs), that constitute solutions to various nonlinear PEL-based micromechanical equations. Importantly, nonlinear excitations do not hybridize with phonons and have been shown to converge in terms of structure and energy to harmonic modes in the limit of low frequency and in the absence of phonon hybridization [13,26–28]. While nonlinear excitations are reliable representations of QLMs, some of them are challenging to compute, as discussed in Ref. [21]. In contrast, pseudoharmonic modes (PHMs)—introduced and discussed in Ref. [21]—are a type of NPM that rely only on the Hessian matrix and do not require computing high-order derivatives of the potential but are still entirely robust against phonon hybridizations. However, there is currently no well-established way to obtain the full distribution of QLMs in glasses by computing NPMs.

Material preparation plays an important role in determining the characteristics of QLMs in glasses and thus directly impacts yielding behavior [29–32]. Building on the resemblance between the spatial structure of QLMs in computer glasses and the typical response of a material to applied local force dipoles, recent work has (i) identified a characteristic energy scale associated with QLMs and (ii) studied the effect of thermal annealing on their abundance, size, and stiffness (Refs. [24,33,34]). These physical properties of QLMs are thought to control ductile and brittle failure in structural glasses [3,24,32]. Further, it was shown in Ref. [3] that structural analyses which rely on the identification of quasilocalized soft modes effectively predict yielding in a variety of model glasses. Accordingly, the identification and characterization of QLMs is very important for the efficacy of several theoretical frameworks that make predictions about the elastoplastic deformation of glasses. For example, STZ theory (Refs. [8,35,36]), soft glassy rheology (SGR) (Refs. [37,38]), and elastoplastic models (Ref. [39]) all rely on the existence of strain-accommodating defects.

Here we study the statistics of a bond-force-response operator $\mathcal{A}$ (referred to in what follows as the "bond operator," for brevity) in the context of the properties of soft excitations in structural glasses. In essence, the linear operator $\mathcal{A}$ describes the local strain induced at one point in the material, which results from applying a unit force dipole elsewhere in the material (see precise definition below). By construction, the contribution of phonons to the bond operator is regular, allowing $\mathcal{A}$ to cleanly reveal the populations of QLMs in model glasses. This operator was first introduced in Ref. [40], where it was used to identify the length scale associated with dipolar response fields in disordered packings of soft disks. Inspired by Refs. [24,40], we thoroughly study the spectral properties of $\mathcal{A}$ (see example in Fig. 1) and highlight its utility in revealing the statistical, spatial, and energetic properties of soft quasilocalized modes in computer glasses.

This paper is structured as follows: Section II details the ensemble of model glasses analyzed in our study; Sec. III defines the bond operator and its properties; Sec. IV presents our scaling predictions and numerical results related to the eigenspectrum of the bond operator, including a discussion of the structural features of bond operator modes and their correspondence to QLMs; Sec. V includes a discussion of our results in the context of recent work.

II. COMPUTER GLASS MODEL

In this work we employ a model computer glass-former which we refer to as inverse power law (IPL) soft spheres, describing the pairwise interaction between particles. Glassy samples consist of N particles in d spatial dimensions interacting via a radially symmetric pairwise interaction potential

given by $u(r_{ij})$, where r_{ij} is the distance between particles i and j. Configurations are prepared with periodic boundary conditions and energy minimized according to the total potential energy $U(\vec{X}) = \sum_{\langle i,j\rangle} u(r_{ij})$, where the sum $\langle i, j\rangle$ runs over all (unique) pairs of interacting particles. We note and emphasize that all spectral analyses presented in our work were calculated for three-dimensional (3D) glasses, while some results were also obtained for 2D glasses for presentational and visualization purposes.

The IPL model is a polydisperse soft spheres model in which particles interact via a purely repulsive pairwise potential $u(r_{ij}) \sim r_{ij}^{-10}$. We cut off and smooth the potential up to two derivatives, as described, e.g., in Ref. [41], where it is also explained how we handled sample-to-sample finite-size effects that emanate from the random drawing of the effective particle sizes from a fat-tailed distribution [42]. The configurations we analyze in this study were first equilibrated at a very broad range of *parent temperatures* T_p using the swap Monte Carlo algorithm [42–44] that allows for extreme supercooling. Glassy configurations were then formed by a conjugate gradient minimization [45] of equilibrium configurations. Our glassy ensembles for each parent temperature T_p consist of 10 000 independent configurations of $N = 2000$ particles in $d = 3$ dimensions. In what follows, all dimensionful observables are reported in simulational units as spelled out in Ref. [41].

III. BOND-FORCE-RESPONSE OPERATOR

A. Definitions and formalism

The bond operator described in detail below is defined in and acts upon the space of interacting pairs or *bonds*. We restrict the discussion to systems for which this *bond space* is a vector space of dimension $N_\mathrm{b} > Nd$, i.e., larger than the system's configuration space, of dimension Nd. Each component in bond space pertains to a single *pair* of interacting particles. For the $N = 2000$, $d = 3$ configurations that are the focus of this study, $N_b \approx \frac{N_z}{2} = 15\,350$, where $z \approx 15.35$ is the approximate average number of pairwise interactions per particle. Below we follow the notation convention that, unless otherwise specified, lowercase variables (such as the pairwise distances r_α between interacting particles) represent bond-space quantities, while uppercase variables (such as particle coordinates $\vec{X}$) represent coordinate-space quantities. Vectors or operators in bond space are indexed with Greek letters, while those in coordinate space are indexed with Latin letters [40,46]. We will use vector and bra-ket notation interchangeably, as it is convenient.

We consider first the change δr_α in the length of the αth bond (consisting of particles i and j), which results from imposing a (small) displacement $\delta\vec{R}$ to particle coordinates. To first order in the imposed displacement's magnitude, the distance r_α is extended or compressed by

$$\delta r_\alpha \simeq \hat{X}_{ij} \cdot (\delta\vec{R}_j - \delta\vec{R}_i), \tag{1}$$

where $\vec{X}_{ij} \equiv \vec{X}_j - \vec{X}_i$ is the difference vector that extends from particle j to particle i, and $\hat{X}_{ij} \equiv \vec{X}_{ij}/|\vec{X}_{ij}|$ is the corresponding unit vector. Equation (1) constitutes a linear transformation from coordinate-space vectors to bond-space vectors via the $N_b \times Nd$-dimensional operator $\mathcal{S}$, defined precisely as

$$\mathcal{S}_{\alpha,k} = \frac{\partial r_\alpha}{\partial \vec{X}_k}. \tag{2}$$

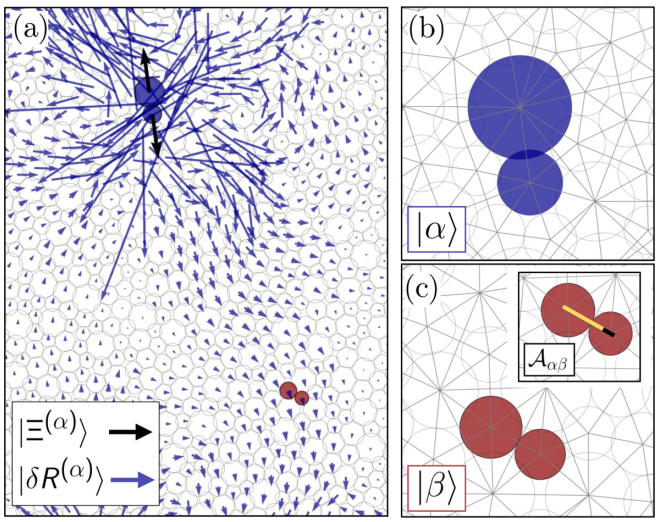

FIG. 2. Bond operator formalism. For an example 2D IPL system: (a) Coordinate-space unit dipole on α, $|\Xi^{(\alpha)}\rangle$ and displacement response $|\delta R^{(\alpha)}\rangle$. (b) Contact network around α. (c) Contact network around β. Inset: $\mathcal{A}_{\alpha\beta}$ measures the change in length of bond β in response to an applied dipolar force on α.

Using this definition, it is convenient to express Eq. (1) for the vector $|\delta r\rangle$ containing the extension or compression of all bonds in the system in bra-ket notation as [47]

$$|\delta r\rangle = \mathcal{S}|\delta R\rangle. \tag{3}$$

Furthermore, to map a bond-space vector to coordinate space, we apply the transpose of $\mathcal{S}$, $\mathcal{S}^T$. For example, if we have a set of interparticle forces $|f\rangle$ and wish to obtain the net force on each particle $|F\rangle$, we simply compute $|F\rangle = \mathcal{S}^T|f\rangle$. References [40,46] discuss the utility of $\mathcal{S}$ and $\mathcal{S}^T$ further. We note that these operators are referred to elsewhere as the compatibility and equilibrium or rigidity matrices respectively [48].

We consider next the change in length of bond β that results from applying a unit dipolar force to the αth bond [40]. A schematic of the relevant objects to this computation in an example 2D system are shown in Fig. 2. We define the bond-space vector $|\alpha\rangle$ to contain all zeros, except for the entry corresponding to the αth bond whose value is unity. A particular bond α is highlighted in panels (a) and (b) of Fig. 2. Operating with $\mathcal{S}^T$ on $|\alpha\rangle$ corresponds to a coordinate-space unit dipole $|\Xi^{(\alpha)}\rangle$ such as that depicted in Fig. 2(a), namely,

$$|\Xi^{(\alpha)}\rangle = \mathcal{S}^T|\alpha\rangle. \tag{4}$$

The (linear) displacement response $|\delta R^{(\alpha)}\rangle$ to such an applied force is simply

$$|\delta R^{(\alpha)}\rangle = \mathcal{M}^{-1}|\Xi^{(\alpha)}\rangle = \mathcal{M}^{-1}\mathcal{S}^T|\alpha\rangle, \tag{5}$$

as shown, for example, in Fig. 2(a). Note that $\mathcal{M}^{-1}$ is here the pseudoinverse of $\mathcal{M}$, which has d translational zero modes. Last, we project the displacement response field $|\delta R^{(\alpha)}\rangle$ onto a dipole constructed on the βth bond [Fig. 2(c)] to obtain the

(α, β) element of the $N_b \times N_b$-dimensional, symmetric, and positive semidefinite bond-force-response operator $\mathcal{A}$. This element is thus given by

$$\mathcal{A}_{\alpha\beta} \equiv \langle \Xi^{(\beta)} | \delta R^{(\alpha)} \rangle = \langle \alpha | \mathcal{S}\mathcal{M}^{-1}\mathcal{S}^T | \beta \rangle, \tag{6}$$

which is schematically shown in the inset of Fig. 2(c), where β is extended by a small amount due to the deformation induced by the applied force on α.

In the discussion that follows, it will be useful to consider an expression for the bond operator in terms of the full eigenmode decomposition of $\mathcal{M}$:

$$\mathcal{A} = \sum_{l=1}^{Nd-d} \frac{\mathcal{S}|\psi_l\rangle\langle\psi_l|\mathcal{S}^T}{\omega_l^2}, \tag{7}$$

where ω_l and $|\psi_l\rangle$ are the eigenfrequencies and corresponding eigenvectors of the Hessian. Particularly, writing $\mathcal{A}$ in this way illustrates how its spectral properties can be understood from those of $\mathcal{M}$. We proceed by noting a few additional features of $\mathcal{A}$ that are relevant to its utility in connecting micromechanical information to overall material behavior.

B. Zero modes of $\mathcal{A}$ are states of self-stress

Bond-space vectors $|\eta\rangle$ that belong to the left null space of $\mathcal{S}$ represent states of self stress (SSS): sets of bond extensions and compressions that do not alter the state of force balance of a system but still introduce mechanical stresses [49]. That is, SSS satisfy $\mathcal{S}^T|\eta\rangle = 0$. Given the definition of $\mathcal{A}$ above [Eqs. (6) and (7)], its zero modes will then be exactly the SSS of the system. For granular packings near the unjamming transition, Maxwell constraint counting implies that $\#\text{SSS} \simeq N\delta z/2$, where δz is the number of excess contacts (past isostaticity) per particle [48]. It follows, given the dimensionality of the bond operator, $N_b \simeq Nz/2$, that the number of nonzero modes of the bond operator is $\sim Nd$.

C. $\mathcal{A}$ within continuum linear elasticity

It is possible to write an exact expression for $\mathcal{A}$ within linear continuum elasticity; however, it is more insightful and less cumbersome to spell out scaling arguments to highlight its expected long-wavelength properties. To this aim, we consider the elastic Green's function $\boldsymbol{\mathcal{G}}(\vec{r}) \sim r^{-(d-2)}$ (in $d > 2$ dimensions) of a linear-elastic, homogeneous, and isotropic solid [50]. The displacement field due to a dipole of length a_0 scales as $a_0 \nabla G \sim a_0 r^{-(d-1)}$. The strain field at distances r from the imposed dipole is thus expected to scale as $a_0^2 \nabla^2 G \sim a_0^2 r^{-d}$. Noticing that $\mathcal{A}$ behaves as the gradient of the displacement field that results from applied force dipoles, we conclude that

$$|\mathcal{A}|(\vec{r}) \sim r^{-d}. \tag{8}$$

The scaling relation given by Eq. (8) was validated numerically in Refs. [13,40]. The r^{-d} decay of interactions is indeed expected for interacting dipoles and forms the basis of lattice models of glassy excitations [51–53], lending further support to the relevance of $\mathcal{A}$ in the present discussion.

IV. SPECTRAL PROPERTIES OF THE BOND OPERATOR

A. Low-frequency contributions to the bond operator

As stated in the Introduction, our goal behind studying the bond operator $\mathcal{A}$ is to propose a systematic route to overcome the hybridization of phonons with QLMs in order to cleanly access the latter. It is convenient to assess the contributions of low-frequency modes of $\mathcal{M}$ to $\mathcal{A}$ by writing $\mathcal{M}^{-1}$ in its eigenbasis as in Eq. (7). In this section, we specifically examine the relative contributions of QLMs and phonons to the construction of $\mathcal{A}$. Intuitively, one can consider these two different contributions to individual elements $\mathcal{A}_{\alpha\beta}$ of the bond operator by comparing the projections of each type of mode (phononic and quasilocalized) onto pairs of coordinate-space dipole vectors $|\Xi^{(\alpha)}\rangle$ and $|\Xi^{(\beta)}\rangle$ via Eqs. (4) and (6). Visually, as depicted in Figs. 1(a) and 1(b), the typical structure of phonons is very dissimilar to that of a local dipole, whereas QLMs highly resemble dipoles and dipolar response fields [Fig. 2(a)].

1. Phonon contributions to $\mathcal{A}$

Here we show that phononic modes of the Hessian have a regular $[\mathcal{O}(1)]$ contribution to $\mathcal{A}$. As stated above, computing elements of $\mathcal{A}$ involves projecting the eigenmodes of the Hessian onto the dipole vectors $|\Xi^{(\alpha)}\rangle$ and $|\Xi^{(\beta)}\rangle$. Since phononic modes of $\mathcal{M}$ are extended plane waves and vary slowly in space, we expect them to have small projections onto local dipoles.

More specifically, consider the following expression for the contributions of phonons $|\Psi_{\text{ph},l}\rangle$ to $\mathcal{A}$:

$$\mathcal{A}_{\text{ph}} = \sum_{\text{ph},l} \frac{\mathcal{S}|\Psi_{\text{ph},l}\rangle\langle\Psi_{\text{ph},l}|\mathcal{S}^T}{\omega_{\text{ph},l}^2}, \tag{9}$$

where $\omega_{\text{ph},l}$ is the eigenfrequency associated with $|\Psi_{\text{ph},l}\rangle$. According to Eqs. (1) and (2), $\mathcal{S}|\Psi_{\text{ph},l}\rangle$ picks up *local* differences of the wavelike mode $|\Psi_{\text{ph},l}\rangle$ and is thus expected to scale as the spatial gradient of $|\Psi_{\text{ph},l}\rangle$, namely, $\mathcal{S}|\Psi_{\text{ph},l}\rangle \sim a_0 \nabla |\Psi_{\text{ph},l}\rangle$. Polarization vectors in phonons vary on the scale of their wavelength, so we conclude that $|\mathcal{S}|\Psi_{\text{ph},l}\rangle| \sim \omega_{\text{ph},l}$. Thus the numerator of Eq. (9) (representing the projection of $\mathcal{M}$ eigenmodes onto dipoles) is on the order of $\omega_{\text{ph},l}^2$ and $\mathcal{A}_{\text{ph}} \sim \mathcal{O}(1)$. We thus conclude that phononic contributions to $\mathcal{A}$ are small compared to those of QLMs, as we show next.

2. QLM contributions to $\mathcal{A}$

Similarly, we now consider the contributions of low-frequency QLMs to $\mathcal{A}$. As observed in Refs. [24,33,34], the structure of QLMs is characterized by a disordered core and algebraically decaying quadrupolar field. In contrast to plane-wave excitations, the disordered core of a QLM features highly nonaffine displacements, which are expected to have large projections onto local dipoles $|\Xi^{(\alpha)}\rangle$. This implies that contributions to $\mathcal{A}$ from QLMs are dominant compared to other excitations. Consider the sum

$$\mathcal{A}_{\text{QLM}} = \sum_{\text{QLM},l} \frac{\mathcal{S}|\Psi_{\text{QLM},l}\rangle\langle\Psi_{\text{QLM},l}|\mathcal{S}^T}{\omega_{\text{QLM},l}^2}, \tag{10}$$

where $|\Psi_{\mathrm{QLM},l}\rangle$ is a QLM with frequency $\omega_{\mathrm{QLM},l}$. Given the propensity of QLMs for extending or compressing pairwise bonds in their cores, we conclude that $\mathcal{S}|\Psi_{\mathrm{QLM},l}\rangle \sim \mathcal{O}(1)$. In contrast to phononic contributions to $\mathcal{A}$, we therefore expect that QLMs of frequency ω_{QLM} contribute terms of order $\omega_{\mathrm{QLM}}^{-2}$ to $\mathcal{A}$.

Importantly, the considerations described above lead us to expect $\mathcal{A}$ to predominantly contain information about disorder-related soft modes in model glasses that are unobscured by phononic modes. Thus we expect that the eigenspectrum of the bond operator should suppress phonon hybridization and cleanly reflect the full distribution of QLMs in the system.

B. Eigenvalue distribution of $\mathcal{A}$

1. High-λ scaling of bond operator spectrum

As previously noted, in the framework of using the harmonic approximation to identify glassy instabilities, one is generally interested in the low-frequency regime of the eigenspectrum of the Hessian, where universal $D(\omega) \sim \omega^4$ scaling is prevalent [22]. Since $\mathcal{A}$ is directly related to the inverse Hessian, in the results that follow we will equivalently be interested in studying the high-eigenvalue scaling of $\mathcal{A}$ [Fig. 1(d)]. Examining Eq. (7), we see that the eigenvalues λ of $\mathcal{A}$ should scale as the inverse squared frequencies of the Hessian: $\lambda \sim \omega^{-2}$. Applying a transformation of variables to convert from $D(\omega) \sim \omega^4$ to some $P(\lambda)$, we obtain

$$P(\lambda) \sim D(\omega(\lambda))|d\omega/d\lambda| \sim \lambda^{-\frac{7}{2}}. \tag{11}$$

More generally, for $D(\omega) \sim \omega^{\gamma}$, we equivalently have $P(\lambda) \sim \lambda^{-\frac{\gamma+3}{2}}$. Thus we have formed a simple scaling prediction for the bond operator eigenspectrum. As we will see, this scaling is robust in the spectrum of $\mathcal{A}$ for a variety of computer glass ensembles. Last, it is important to note that the transformation of variables performed here preserves the prefactor A_{g} of the $\sim\omega^4$ scaling [i.e., $D(\omega) = A_{\mathrm{g}}\omega^4$], and so we expect to observe $P(\lambda) \sim A_{\mathrm{g}}\lambda^{-7/2}$, as discussed extensively below.

2. Results: Bond operator spectrum

To study the full distribution of disorder-related modes in our model glasses, we computed and diagonalized $\mathcal{A}$ for 10 000-configuration ensembles as noted above, prepared in $d = 3$ with $N = 2000$ particles at four different parent temperatures $T_p \in \{0.32, 0.45, 0.60, 1.00\}$. Figure 3(a) shows the distributions of eigenvalues for these samples. The high-λ regime robustly displays the $\lambda^{-7/2}$ scaling predicted in Eq. (11), especially for less deeply annealed glasses such as those with $T_{\mathrm{p}} \gtrsim 0.5$. We also observe that the prefactor A_{g} associated with the $\lambda^{-7/2}$ power law increases with larger T_{p}. This is expected, as previous work has shown that the overall number of QLMs depends strongly on equilibrium parent temperature [23,24,33]. We will address this point thoroughly to follow.

The clarity of the $P(\lambda) \sim \lambda^{-7/2}$ scaling observed here contrasts typical $D(\omega) \sim \omega^4$ spectra, which are often obscured by the presence of phononic excitations. Phonons in the spectrum of $\mathcal{M}$ in finite-size solids introduce a system-size dependence that does not exist in that of $\mathcal{A}$. For example, the typical

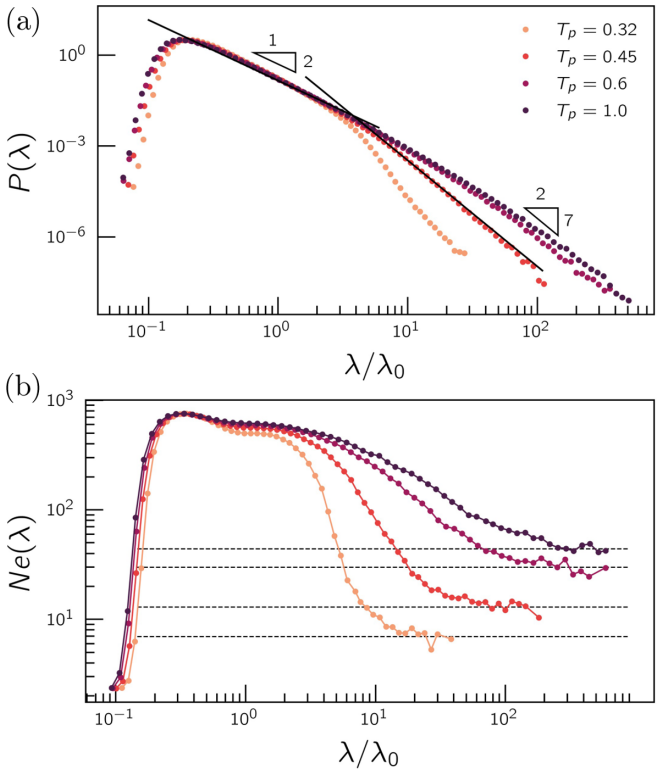

FIG. 3. Spectrum of bond operator for varying material preparation protocols. (a) Distribution of $\mathcal{A}$ eigenvalues for four different T_{p}. Lighter colors (bottom) represent deeper annealing. The scale triangles depict the predicted high-λ $P(\lambda) \sim \lambda^{-7/2}$ power law and mid-λ $P(\lambda) \sim \lambda^{-2}$ scaling respectively. (b) Participation ratio of particle force modes multiplied by N as a function of λ for varying T_{p}, color scale as in (a). We use the plateau values of Ne in the high-λ regime to extract QLM length scales ξ from $\mathcal{A}$ modes.

frequency of the first phonons in a solid of size L is $\omega_{\mathrm{ph}} = 2\pi c_s/L$ where c_s is the shear wave speed. In finite-size solids the lowest-frequency phonons usually appear in quantized bands [19], rendering $D(\omega)$ explicitly system-size dependent. This can be seen in Figs. 1(c) and 1(d), as there is a clear phonon peak in the spectrum of the Hessian but not in that of the bond operator. The spectrum of $\mathcal{A}$ is thus system-size independent as demonstrated in Appendix B. We emphasize that the scaling behaviors of $D(\omega)$ and $P(\lambda)$ are equivalent, but the bond operator recovers the result more cleanly than the Hessian alone by virtue of its ability to dehybridize phononic and quasilocalized soft modes of the system.

We finally note that, in the mid-λ regime of the bond operator spectrum, we observe clear $P(\lambda) \sim \lambda^{-2}$ scaling independent of T_{p}, which is reminiscent of $D(\omega) \sim \omega$ scaling observed at intermediate frequencies in the density of states of lattice models for interacting glassy QLMs [51–53]. This observation further elucidates $\mathcal{A}$'s utility for identifying and analyzing nonphononic excitations.

3. Results: Localization of high-λ eigenmodes

An important feature to observe in disordered solids is the presence of a length scale associated with QLM's core size [24]. Toward this goal, we analyze the participation ratio

profile of bond operator eigenmodes as a function of their associated eigenvalues λ. Specifically, we use coordinate-space modes derived from high-λ modes of the bond operator (which we will define as "particle force modes" and discuss in detail below) to compute participation via

$$e(\vec{F}) \equiv \frac{\left(\sum_i \vec{F}_i \cdot \vec{F}_i\right)^2}{N \sum_i (\vec{F}_i \cdot \vec{F}_i)^2}, \tag{12}$$

where the sums are over particle indices and $\vec{F}_i$ is the d-dimensional vector prescribing the force on i in the aforementioned coordinate-space mode. This analysis is summarized in Fig. 3(b), which shows $Ne(\lambda)$ for the same group of glass ensembles as in Fig. 3(a). The low-λ regime is characterized by very localized modes that quickly increase in participation with growing λ. These correspond to high-stiffness excitations such as Eshelby-like deformations on a small number of particles, transitioning to more extended modes that apply small forces to many particles. See Appendix A for further details regarding the participation of intermediate-λ $\mathcal{A}$ eigenmodes.

More interestingly, for high λ, the coordinate-space $\mathcal{A}$ modes become localized and strongly resemble QLMs, reaching a plateau in participation as indicated by the horizontal lines in Fig. 3(b). By identifying the participation for which the Ne profile reaches 15% above its plateau value, we extract the typical number n of particles that participate in QLM-like excitations obtained from $\mathcal{A}$, usually ∼10s of particles. Each n thus gives a characteristic QLM length scale ξ via

$$\xi = a_0 n^{\frac{1}{d}}, \tag{13}$$

where $a_0 \equiv (V/N)^{1/d}$ is a characteristic interparticle distance. As we will discuss, the length scale associated with high-λ eigenmodes decreases significantly with deeper annealing, in agreement with other methods for investigating the interplay of material preparation and QLM properties [24,33,34].

C. Eigenvectors of $\mathcal{A}$ and their connection to QLMs

1. Relevant modes and spatial decay

In the discussion that follows, we will define a family of modes that can be derived from the bond operator and briefly formulate scaling arguments that predict their characteristic spatial decay.

a. Bond force modes. By diagonalizing $\mathcal{A}$ we obtain its eigenvectors, which we will refer to as *bond force modes*, denote $|f\rangle$, and interpret as fields of bond extension and compression forces. Bond force modes are N_b-dimensional and can also be understood as fields that describe local strain on the scale of particle bonds.

b. Particle force modes. To instead study bond force modes in coordinate space, we compute *particle force modes* $|F\rangle$, via $|F\rangle = \mathcal{S}^T|f\rangle$. Particle force modes are Nd-dimensional and can be interpreted as applied forces on each particle that constitute an equivalent deformation to the corresponding bond force mode.

c. Particle displacement modes. Recall that harmonic vibrational modes (of the Hessian) and QLMs are typically viewed as putative displacement fields about a mechanically stable configuration that can represent structural instabilities or loci of potential plastic yielding. Thus we compute Nd-dimensional *particle displacement modes* $|D\rangle$ by applying the inverse Hessian to particle force modes: $|D\rangle = \mathcal{M}^{-1}\mathcal{S}^T|f\rangle$.

d. Pseudoharmonic displacement modes. As previously noted, several recent works (Refs. [3,13,21,26–28]) have formulated and studied NPMs and PHMs as faithful representations of structural instabilities in model glasses. Significantly, these modes resist hybridization with phononic excitations, which is a notable shortcoming of traditional harmonic vibrational modes [21]. Here we focus on PHMs as a benchmark for using modes of the bond operator to identify QLMs in model glasses. We first provide background information about formulating PHMs and then define the corresponding PHMs to particle displacement modes and particle force modes.

Pseudoharmonic modes (PHMs) $\vec{\pi}$ rely only on the harmonic approximation of the energy and can be obtained by minimizing the cost function [21]:

$$\mathcal{C}(\vec{z}) = \frac{(\mathcal{M} : \vec{z}\vec{z})^2}{\sum_{\langle i,j\rangle} (\vec{z}_{ij} \cdot \vec{z}_{ij})^2}, \tag{14}$$

with respect to the field $\vec{z}$. Here the notation $\mathcal{M} : \vec{z}\vec{z}$ denotes a double contraction of the field $\vec{z}$ with the Hessian, the sum in the denominator is over all interacting particle pairs ij, and $\vec{z}_{ij} = \vec{z}_j - \vec{z}_i$. Fields $\vec{\pi}$ associated with low-lying minima of $\mathcal{C}(\vec{z})$ satisfy $\partial\mathcal{C}/\partial\vec{z}|_{\vec{\pi}} = \mathbf{0}$; they feature small stiffness [given by the numerator of Eq. (14)] and a small participation ratio (thereby maximizing the denominator) [21]. Thus, long-wavelength plane waves are suppressed, and disorder-related excitations (QLMs) are clearly identified. In practice, PHMs can be obtained by starting with an initial guess $\vec{z}_0$ and minimizing the cost function via a routine such as conjugate gradient. This highlights a major benefit of the bond operator approach compared to nonlinear frameworks such as PHMs, namely, it does not require obtaining relevant initial guesses to identify each QLM, as explained in [13,21,26]. Conversely, examining the high-λ regime of the bond operator spectrum provides direct access to the population of QLMs in glassy samples and requires no ad hoc inputs, as we show below. For further information regarding PHMs, see Refs. [21,27].

Now, if we use a particle displacement mode as the initialization for computing a PHM, $\vec{z}_0 \to |D\rangle$, we obtain $|D_{\mathrm{PH}}\rangle$, a Nd-dimensional *pseudoharmonic displacement mode* that corresponds to $|D\rangle$. In other words, $|D_{\mathrm{PH}}\rangle$ should be viewed as $|D\rangle$ with obscuring de-localized features removed by the PHM protocol.

e. Pseudoharmonic force modes. The forces that result from displacing the system via $|D_{\mathrm{PH}}\rangle$ are simply given by $|F_{\mathrm{PH}}\rangle = \mathcal{M}|D_{\mathrm{PH}}\rangle$, which we thus define as *pseudoharmonic force modes*. We reemphasize that in the analysis presented here we will use comparisons between $|D\rangle$ and $|D_{\mathrm{PH}}\rangle$ (and $|F\rangle$ and $|F_{\mathrm{PH}}\rangle$) to determine how close particle displacement and particle force modes are to their pure QLM counterparts.

f. Spatial decay. In general, it has been noted in Refs. [18,26,28] that the spatial structure of QLMs is characterized by a disordered (dipole-response-like) core, decorated by a decaying field that scales as $\sim r^{-(d-1)}$ where r is the distance from the core. Since $|D_{\mathrm{PH}}\rangle$ is a faithful representation of a QLM, we expect that its decay will match this profile. We

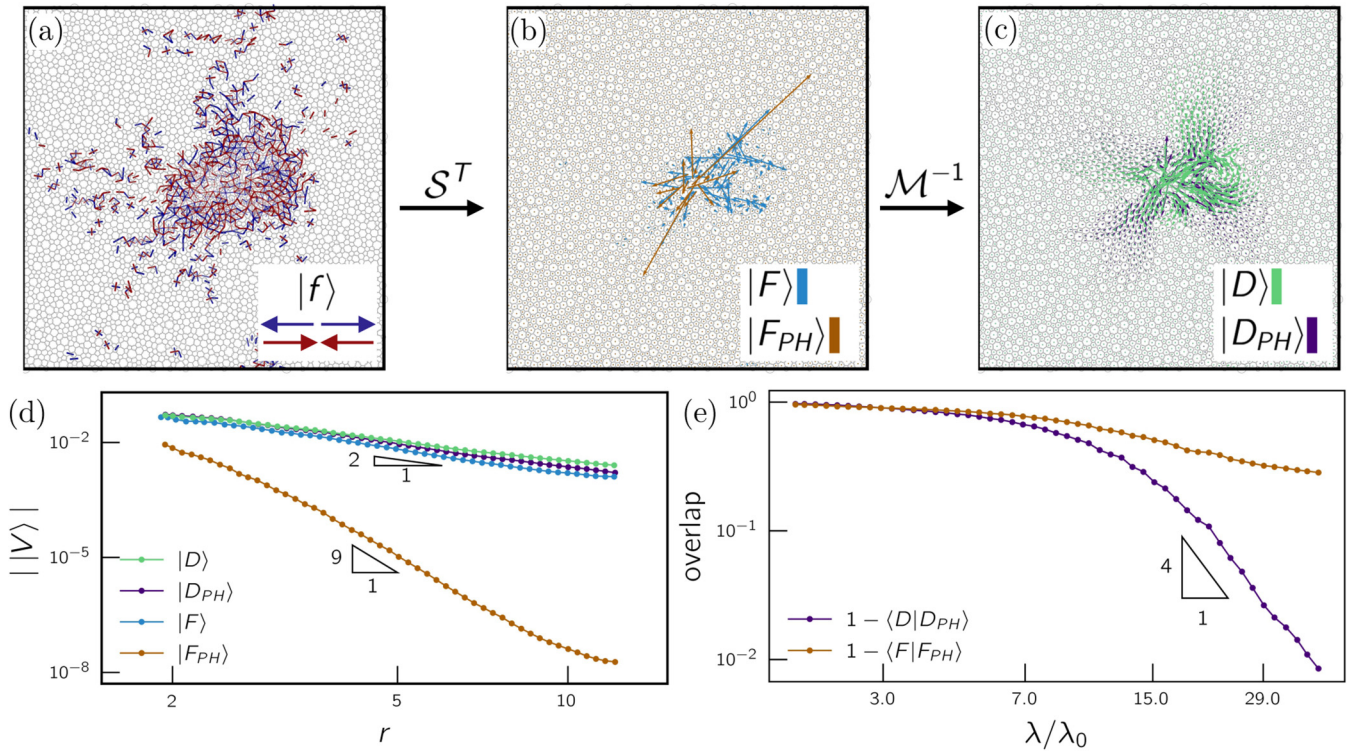

FIG. 4. Eigenmodes of $\mathcal{A}$ and their correspondence to PHMs. (a) High-λ bond force mode $|f\rangle$ obtained by diagonalizing $\mathcal{A}$. Red-colored bonds represent extension, and blue-colored bonds represent compression. Line opacity and thickness are adjusted to reflect the magnitude of extension or compression, and we color only the top 10% (in magnitude) of bonds. (b) Particle force mode $|F\rangle$ (blue) corresponding to the bond force mode in (a) and related pseudoharmonic force mode $|F_{\rm PH}\rangle$ (orange). (c) Particle displacement mode $|D\rangle$ (green) corresponding to the particle force mode in (b) and related pseudoharmonic displacement mode $|D_{\rm PH}\rangle$ (purple). (d) Spatial decay profiles of polarization vector magnitudes as a function of distance from disordered core. Colored points for each type of mode are the same as in (a)–(c). (e) Convergence of particle displacement and particle force modes to their corresponding PHMs. The results shown in (d) and (e) are for our ensemble of 3D IPL glasses, whereas (a)–(c) are presented in 2D for ease of visualization.

can similarly examine the structure of $|F_{\rm PH}\rangle$. Using arguments related to the definition of pseudoharmonic modes as fields minimizing Eq. (14) (see Refs. [21,28]), we predict that pseudoharmonic force modes decay spatially as the cube of the gradient of $|D_{\rm PH}\rangle$. Thus, $||F_{\rm PH}\rangle| \sim r^{-9}$ for $d = 3$.

2. *Results: Spatial structure and correspondence to PHMs*

As discussed above, we can use the formalism of the bond operator to study a family of disorder-related modes that represent structural precursors to plasticity in model glasses. Here we discuss the resemblance of coordinate-space representations of bond operator eigenvectors to their corresponding PHMs. For ease of visualization, Figs. 4(a)–4(c) show high-λ modes derived from the bond operator in a representative 2D IPL system with $N = 4096$ particles. The bond force mode $|f\rangle$ depicted in Fig. 4(a) shows a field of extensions and compressions localized on a core of bonds. We note here that bond force modes can be interpreted as local strain fields due to the bond operator's relationship to the elastic Green's function as described above. This set of bond forces translates to a particle force mode $|F\rangle$ and pseudoharmonic force mode $|F_{\rm PH}\rangle$ that are similarly localized, as shown in Fig. 4(b). Figure 4(c) shows the particle displacement mode $|D\rangle$ and pseudoharmonic displacement mode $|D_{\rm PH}\rangle$ that constitute the (linear) response of the system to the applied forces $|F\rangle$ and $|F_{\rm PH}\rangle$ respectively. Significantly, we see that $|D\rangle$ closely resembles $|D_{\rm PH}\rangle$. These displacement modes illustrate typical features of QLMs: low-stiffness excitations that localize on a distinct group of particles and have spatial structures characterized by a disordered core and radially decaying field.

We will now quantify the spatial structure and the convergence of $|F\rangle$ and $|D\rangle$ to their pseudoharmonic counterparts. Figure 4(d) shows the decay profiles of the coordinate-space modes discussed above. We computed the running median of the magnitude of polarization vectors on particles in each mode as a function of radius r away from the core of the mode, where the core position is approximated by the location of the particle with the largest polarization vector magnitude. The results were averaged over 1000 high-λ modes from 3D, IPL systems with $N = 2000$ particles, and $T_p = 0.45$. As is expected for QLMs, $|D\rangle$ and $|D_{\rm PH}\rangle$ decay spatially as $\sim r^{-(d-1)} = r^{-2}$ in 3D [26]. More surprisingly, $|F\rangle$ falls off with the same scaling, indicating that the forces prescribed by the high-λ bond operator mode behave similarly to their corresponding displacements. This behavior of $|D\rangle$ and $|F\rangle$ is reminiscent of low-frequency harmonic modes, where the force and displacement modes are in the same direction. Conversely, $|F_{\rm PH}\rangle$ decays much faster than $|F\rangle$: $||F_{\rm PH}\rangle| \sim r^{-9}$, in agreement with

our prediction. This difference in spatial decay is consistent with the clear variation in general structure between the two types of particle force modes. Significantly, we have shown that high-λ modes of the bond operator are robust representations of phonon-free QLMs in model glasses, highlighting $\mathcal{A}$ as a reliable source of useful micromechanical information.

Figure 4(e) shows the convergence of $|D\rangle$ to the structure of $|D_{\mathrm{PH}}\rangle$ and $|F\rangle$ to $|F_{\mathrm{PH}}\rangle$, respectively, as a function of λ. We compute and average the overlap of these pairs of modes (simply defined as $1-\langle V|V_{\mathrm{PH}}\rangle$ for $V \to D, F$) for the same data as in Fig. 4(d). In the limit of large λ, $|D\rangle$ converges quickly as $\sim\lambda^{-4}$ to its PHM, whereas $|F\rangle$ does not. This suggests that small variations between $|D\rangle$ and $|D_{\mathrm{PH}}\rangle$ give rise to large differences in the according force modes. In other words, there is some allowable variation in sets of applied forces that could still give rise to QLM-like displacement fields.

D. Effect of thermal annealing on QLM properties reflected by $\mathcal{A}$

The results presented in Fig. 3 showed that the statistics of QLMs in glassy samples can be cleanly observed in the $\mathcal{A}$ spectra for a variety of T_{p}. We emphasize that these features are generically difficult to extract from the density of modes of the Hessian due to system-size and hybridization effects. As discussed thoroughly in Ref. [24], there are three notable QLM features that vary drastically with deeper annealing (decreasing T_{p}): depletion of the density $\mathcal{N}$ of disorder modes in the system, shrinking of the QLM length scale ξ, and stiffening of the potential energy landscape (typically measured by the frequency ω_{g} of soft modes). Our results from analysis of the bond operator robustly support these claims. By fitting our distributions of $\mathcal{A}$ eigenvalues from Fig. 3(a) to the scaling relation $P(\lambda)\sim A_{\mathrm{g}}\,\lambda^{-7/2}$ in the large eigenvalue regime associated with QLMs, we obtain the values of the prefactors A_{g} which vary with T_{p}. As is discussed extensively in Ref. [24], an integral over the density of modes (or bond operator eigenvalues) shows that A_{g} encodes important information about both the density $\mathcal{N}$ and stiffness ω_{g} of glassy QLMs.

In their recent work, Rainone et al. used a characteristic QLM frequency ω_{g} extracted from the average response of glassy samples to applied dipolar forces to disentangle contributions to the $D(\omega)\sim\omega^4$ prefactor by $\mathcal{N}$ and a multiplicative factor of ω_{g}^{-5} that arises from integrating the density of modes over a finite range [24]. The authors then study the effect of annealing on QLM depletion by measuring $\mathcal{N}$ as a function of T_{p}. Figure 5 shows our extracted $P(\lambda)$ prefactors as a function of parent temperature overlaid on the data reproduced from [24,33]. To remove the overall scale that differs between the two datasets, we divide the $P(\lambda)$ prefactors by that of the high-T_{p} ensemble and report values of the ratio $R_{A_{\mathrm{g}}}=A_{\mathrm{g}}/A_{\mathrm{g},\mathrm{T_p}\to\infty}$. As we see, there is good agreement between the observed trend in both studies. Thus the bond operator spectrum is a reliable way to recover A_{g} as a function of annealing. Notably, the values of A_{g} vary by three orders of magnitude within the range of T_{p} that we explored.

Next, we examine the effect of annealing on the QLM length scales extracted from the participation plateaus in Fig. 3(b) via Eq. (13). We compare these lengths, shown in the inset of Fig. 5, to those reported in Ref. [24]. Rainone et al. computed their QLM length scales for each sample parent temperature via the relation $\xi=2\pi c_s/\omega_{\mathrm{g}}$, where ω_{g} is the dipolar response-derived characteristic frequency and c_s is the shear wave speed. Again, we divide the ξ values by the high temperature case and report the ratio $R_\xi \equiv \xi/\xi_{T_p\to\infty}$ for ease of comparison. Interestingly, despite seemingly different approaches for identifying the QLM length scales, our results agree quite well. These results further elucidate the utility of the bond operator to provide important insight into the properties of glassy QLMs a function of material preparation and memory.

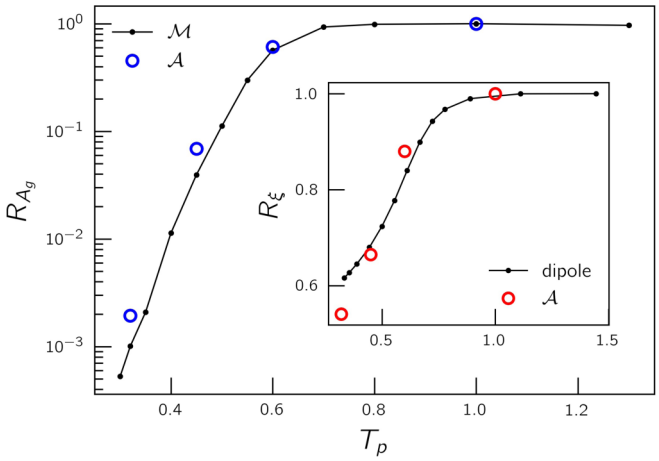

FIG. 5. Effect of thermal annealing on A_{g} and ξ. Prefactor ratios $R_{A_{\mathrm{g}}}$ extracted from $P(\lambda)$ distributions in Fig. 3(a) as a function of parent temperature (open blue circles), overlaid on data reproduced from Ref. [24] (black connected dots). The inset shows the QLM length scale ratio R_ξ extracted from the participation plateaus in Fig. 3(b) as a function of parent temperature (open red circles), also overlaid on data from Ref. [24] (black connected dots).

V. SUMMARY, DISCUSSION, AND OUTLOOK

Overall, we have shown that the bond force response operator, $\mathcal{A}$, is a powerful object that cleanly provides insight into many statistical and structural features of glassy instabilities. The operator acts on bond-space vectors and gives the deformation induced in particle bonds in response to a set of applied compressions and extensions. We provide intuition and numerical evidence for why a bond-space perspective on instabilities in disordered solids is valuable. Contrasting the spectrum of vibrational modes of the Hessian, which is complicated by finite-size effects and hybridization processes, the bond operator cleanly captures the statistics of disorder-related modes in model glasses. In other words, we have shown that the spectrum of $\mathcal{A}$ is system-size independent and appears to efficiently dehybridize low-frequency QLMs from phononic excitations. The high-eigenvalue scaling of the bond operator that we have measured, $P(\lambda)\sim\lambda^{-7/2}$, is equivalent to the universal low-frequency $D(\omega)\sim\omega^4$ law [22–25]. We explored the spectral properties of the bond operator and

highlighted the direct correspondence between its high-eigenvalue eigenmodes and QLMs. By examining ensembles of swap Monte Carlo IPL model glasses, we further explored the effect of deep annealing on QLM properties. Reliably identifying and understanding glassy defects is an important step toward building a comprehensive theory of the rheology of disordered materials.

As we have discussed, existing frameworks such as NPMs and PHMs have successfully identified populations of QLMs in disordered solids [21,27]. Since NPMs require the computation of high-order derivatives of the potential energy of the system, and both methods require initial guesses to find representations of QLMs via minimization of a nonlinear cost function, a relative strength of $\mathcal{A}$ is that it provides direct access to the full spectrum of phonon-free QLMs. We have shown that particle displacement modes $|D\rangle$, derived directly from high-λ modes of the bond operator, quickly converge structurally to their corresponding PHMs.

Previous work used the response of disordered packings to local force perturbations (applied dipolar extension) as well as the density of harmonic modes $D(\omega)$ to determine the annealing dependence of QLM depletion, shrinking, and stiffening [24,33,34]. In our analysis of the bond operator, we measured $P(\lambda)$ prefactors A_g as a function of parent temperature T_p and found good agreement with the results of Ref. [24]. Additionally, we used the high-λ plateau observed in the participation profile of bond operator modes to identify a length scale ξ that decreases with deeper annealing. Conveniently, by computing only the bond operator, we gain access to spatial, mechanical, and statistical properties of glassy excitations that are important to popular theoretical frameworks such as STZ theory, SGR, and elastoplastic models.

We note that computing the bond operator for large systems remains challenging, as fully diagonalizing the Hessian is computationally intensive. However, the bond operator is a useful tool for analyzing glassy instabilities in small systems, for example, packings of a few thousand particles whose typical interaction range does not exceed a few particle diameters. Still, it may be possible to extract the same information that we have presented here using approximations of the bond operator, such as from a partial sum over the low-frequency modes of the Hessian as in Eq. (7) or a cutoff on the interparticle interaction range in systems where long-range interactions may not be important to the overall micromechanics; these are avenues for future work. Furthermore, the bond operator could provide valuable insight into the structure of a variety of glass-forming models such as Stillinger-Weber or sticky spheres [21,54].

In this work we focused solely on annealing as a preparation protocol that effects the mechanical features of the resulting material. However, given the bond operator's strength as a tool for studying QLMs and their properties, it would be illuminating to utilize it in future analyses of a broad range of computer glass ensembles. In particular, thoroughly studying the (phonon-free) vibrational spectra of loosely compressed particle packings near the unjamming transition would help inform current theories for glassy instabilities and rigidity. Such a study could help answer open questions about distinct populations of extended and localized low-frequency vibrations in low-coordination solids.

ACKNOWLEDGMENTS

E.L. acknowledges support from the NWO (Vidi Grant No. 680-47-554/3259). J.A.G. and M.L.M. acknowledge support from the Simons Foundation through Grant No. 454947 and the National Science Foundation through Grant No. NSF-DMR-1951921. D.R. acknowledges support from the Simons Foundation for the "Cracking the Glass Problem Collaboration" Award No. 348126.

APPENDIX A: INTERMEDIATE-λ MODES OF $\mathcal{A}$

Similarly to Fig. 3(b) in the main text, in Fig. 6(a) we show the participation ratio (multiplied by system size) as a function of λ for a small ensemble of particle force modes and particle displacement modes derived from eigenvectors of $\mathcal{A}$. The data presented here is from ∼150 IPL glasses in 2D with $N = 4096$ particles and $T_\mathrm{p} = 0.7$. We see that the participation profiles for the two types of modes vary by an overall factor for most of the range in λ, but the trends and tendency toward a plateau are the same. In panels (b)–(d) and (e)–(g) of Fig. 6, we show example $|D\rangle$ and $|F\rangle$ modes, respectively, that lie

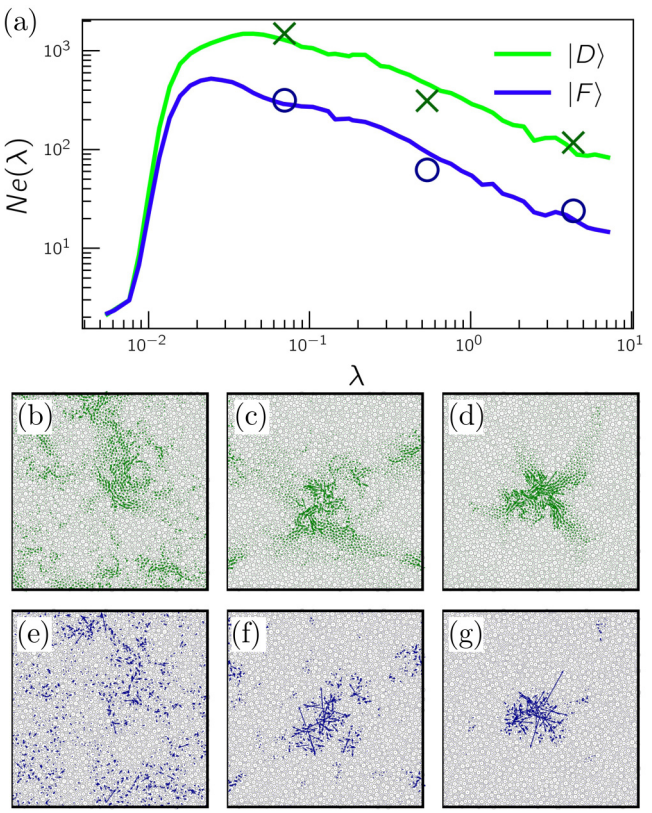

FIG. 6. (a) Participation ratio as a function of $\mathcal{A}$ eigenvalue λ for particle force modes (blue, bottom) and particle displacement modes (green, top). Markers represent the participations and eigenvalues associated with the sample $|D\rangle$ and $|F\rangle$ modes in (b)–(g), which are arranged in the same order. (b)–(d) Particle displacement modes corresponding to the profile in (a), arranged from low to high λ from left to right. (e)–(g) Particle force modes corresponding to the profile in (a), arranged from low to high λ from left to right.

in the intermediate-λ regime of the spectrum. Approaching higher λ, the modes begin to resemble QLMs.

APPENDIX B: $\mathcal{A}$ SPECTRUM AND SYSTEM-SIZE DEPENDENCE

To show that $\mathcal{A}$'s eigenspectrum is independent of system size, we analyzed a variety of 3D 50:50 bidisperse harmonic sphere packings prepared at pressure $p=0.1$ expressed in simulational units. The ratio of diameters of large and small spheres is set to 1.4. The harmonic spheres interact via the pairwise potential

$$u(r_{ij}) = \begin{cases} \frac{1}{2}k(r_{ij} - l_{0,ij})^2, & r_{ij} \leqslant l_{0,ij} \\ 0, & r_{ij} > l_{0,ij} \end{cases}, \qquad \text{(B1)}$$

where k (set to unity) is a spring constant associated with the bond (particle pair) ij and $l_{0,ij}$ is the bond rest length. All $l_{0,ij}$ are set to the sum of the radii of particles i and j, $l_{0,ij}=d_i+d_j$. We created glasses at the desired target pressure using the FIRE energy minimization algorithm [55]. See Ref. [41] (discussion of Hertzian sphere packing preparation) for further details of the implementation. Here we analyze 1000 independent configurations for each $N \in \{1000, 2000, 4000\}$.

By comparing panels (a) and (b) of Fig. 7, we see that $P(\lambda)$ is independent of system size while $D(\omega)$ has phonon peaks in the spectrum that change frequency as a function of simulation box size L (such a peak is also clearly visible in Fig. 1 in the main text). This emphasizes the utility of the bond operator for investigating the phonon-free spectrum of QLMs in model glasses.

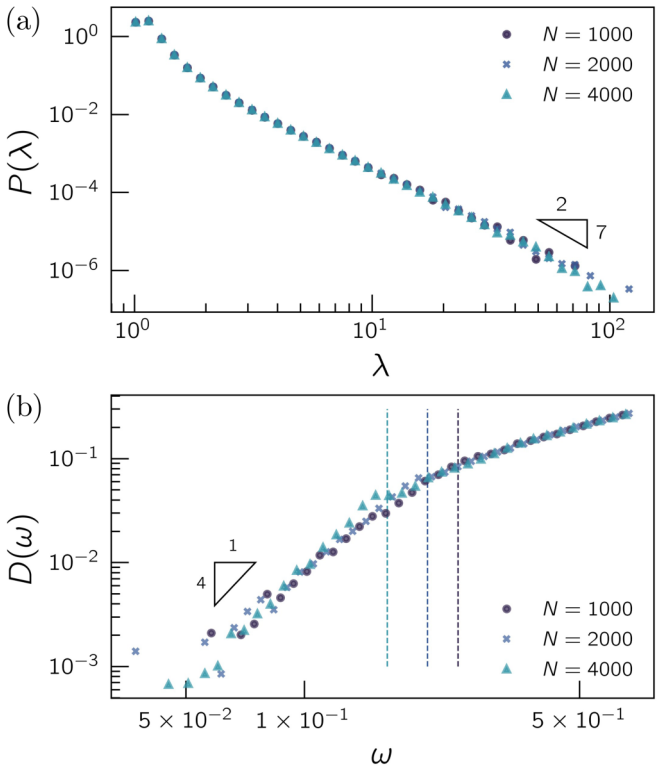

FIG. 7. $P(\lambda)$ and $D(\omega)$ distributions for ensembles of harmonic sphere packings. Spectra for varying system sizes are represented with different shapes and colors of marker as shown. (a) Full $P(\lambda)$ spectrum, where the scale triangle represents $P(\lambda) \sim \lambda^{-7/2}$ scaling. (b) The low-frequency $D(\omega)$ is shown to emphasize the presence of phonons. The scale triangle represents $D(\omega) \sim \omega^4$ scaling. Dashed vertical lines depict the lowest phonon frequency given by $\omega_{\text{ph}} = 2\pi c_s/L$ where corresponding peaks are visible.

[1] E. D. Cubuk, R. J. S. Ivancic, S. S. Schoenholz, D. J. Strickland, A. Basu, Z. S. Davidson, J. Fontaine, J. L. Hor, Y.-R. Huang, J. Li, R. Riggleman, K. T. Turner, A. G. Yodh, D. S. Gianola, A. J. Liu *et al.*, Structure-property relationships from universal signatures of plasticity in disordered solids, Science **358**, 1033 (2017).

[2] L. Berthier and G. Biroli, Theoretical perspective on the glass transition and amorphous materials, Rev. Mod. Phys. **83**, 587 (2011).

[3] D. Richard, M. Ozawa, S. Patinet, E. Stanifer, B. Shang, S. A. Ridout, B. Xu, G. Zhang, P. K. Morse, J.-L. Barrat, L. Berthier, M. L. Falk, P. Guan, A. J. Liu, K. Martens, S. Sastry, D. Vandembroucq, E. Lerner, and M. L. Manning, Predicting plasticity in disordered solids from structural indicators, Phys. Rev. Mater. **4**, 113609 (2020).

[4] R. C. Zeller and R. O. Pohl, Thermal conductivity and specific heat of noncrystalline solids, Phys. Rev. B **4**, 2029 (1971).

[5] F. Varnik, L. Bocquet, and J.-L. Barrat, A study of the static yield stress in a binary Lennard-Jones glass, J. Chem. Phys. **120**, 2788 (2004).

[6] H. J. Barlow, J. O. Cochran, and S. M. Fielding, Ductile and Brittle Yielding in Thermal and Athermal Amorphous Materials, Phys. Rev. Lett. **125**, 168003 (2020).

[7] A. Argon, Plastic deformation in metallic glasses, Acta Metall. **27**, 47 (1979).

[8] M. L. Falk and J. S. Langer, Dynamics of viscoplastic deformation in amorphous solids, Phys. Rev. E **57**, 7192 (1998).

[9] C. Scalliet, L. Berthier, and F. Zamponi, Nature of excitations and defects in structural glasses, Nat. Commun. **10**, (2019).

[10] S. Patinet, D. Vandembroucq, and M. L. Falk, Connecting Local Yield Stresses with Plastic Activity in Amorphous Solids, Phys. Rev. Lett. **117**, 045501 (2016).

[11] P. Morse, S. Wijtmans, M. van Deen, M. van Hecke, and M. L. Manning, Differences in plasticity between hard and soft spheres, Phys. Rev. Res. **2**, 023179 (2020).

[12] M. L. Manning and A. J. Liu, Vibrational Modes Identify Soft Spots in a Sheared Disordered Packing, Phys. Rev. Lett. **107**, 108302 (2011).

[13] L. Gartner and E. Lerner, Nonlinear plastic modes in disordered solids, Phys. Rev. E **93**, 011001(R) (2016).

[14] Z. Schwartzman-Nowik, E. Lerner, and E. Bouchbinder, Anisotropic structural predictor in glassy materials, Phys. Rev. E **99**, 060601(R) (2019).

[15] M. Goldstein, Viscous liquids and the glass transition: A potential energy barrier picture, J. Chem. Phys. **51**, 3728 (1969).

[16] D. L. Malandro and D. J. Lacks, Relationships of shear-induced changes in the potential energy landscape to the mechanical properties of ductile glasses, J. Chem. Phys. **110**, 4593 (1999).

[17] C. Maloney and A. Lemaître, Universal Breakdown of Elasticity at the Onset of Material Failure, Phys. Rev. Lett. **93**, 195501 (2004).

[18] E. Lerner, G. Düring, and E. Bouchbinder, Statistics and Properties of Low-Frequency Vibrational Modes in Structural Glasses, Phys. Rev. Lett. **117**, 035501 (2016).

[19] E. Bouchbinder and E. Lerner, Universal disorder-induced broadening of phonon bands: From disordered lattices to glasses, New J. Phys. **20**, 073022 (2018).

[20] E. Lerner, Finite-size effects in the nonphononic density of states in computer glasses, Phys. Rev. E **101**, 032120 (2020).

[21] D. Richard, G. Kapteijns, J. A. Giannini, M. L. Manning, and E. Lerner, Simple and Broadly Applicable Definition of Shear Transformation Zones, Phys. Rev. Lett. **126**, 015501 (2021).

[22] G. Kapteijns, E. Bouchbinder, and E. Lerner, Universal Nonphononic Density of States in 2D, 3D, and 4D Glasses, Phys. Rev. Lett. **121**, 055501 (2018).

[23] L. Wang, A. Ninarello, P. Guan, L. Berthier, G. Szamel, and E. Flenner, Low-frequency vibrational modes of stable glasses, Nat. Commun. **10**, 26 (2019).

[24] C. Rainone, E. Bouchbinder, and E. Lerner, Pinching a glass reveals key properties of its soft spots, Proc. Natl. Acad. Sci. USA **117**, 5228 (2020).

[25] D. Richard, K. González-López, G. Kapteijns, R. Pater, T. Vaknin, E. Bouchbinder, and E. Lerner, Universality of the Nonphononic Vibrational Spectrum Across Different Classes of Computer Glasses, Phys. Rev. Lett. **125**, 085502 (2020).

[26] L. Gartner and E. Lerner, Nonlinear modes disentangle glassy and Goldstone modes in structural glasses, SciPost Phys. **1**, 016 (2016).

[27] G. Kapteijns, D. Richard, and E. Lerner, Nonlinear quasilocalized excitations in glasses. I. True representatives of soft spots, Phys. Rev. E **101**, 032130 (2020).

[28] E. Lerner, The micromechanics of nonlinear plastic modes, Phys. Rev. E **93**, 053004 (2016).

[29] J. J. Lewandowski, Effects of annealing and changes in stress state on fracture toughness of bulk metallic glass, Mater. Trans. **42**, 633 (2001).

[30] C. H. Rycroft and E. Bouchbinder, Fracture Toughness of Metallic Glasses: Annealing-Induced Embrittlement, Phys. Rev. Lett. **109**, 194301 (2012).

[31] M. Ozawa, L. Berthier, G. Biroli, A. Rosso, and G. Tarjus, Random critical point separates brittle and ductile yielding transitions in amorphous materials, Proc. Natl. Acad. Sci. USA **115**, 6656 (2018).

[32] D. Richard, E. Lerner, and E. Bouchbinder, Brittle-to-ductile transitions in glasses: Roles of soft defects and loading geometry, MRS Bulletin (2021), doi:10.1557/s43577-021-00171-8.

[33] E. Lerner and E. Bouchbinder, A characteristic energy scale in glasses, J. Chem. Phys. **148**, 214502 (2018).

[34] C. Rainone, E. Bouchbinder, and E. Lerner, Statistical mechanics of local force dipole responses in computer glasses, J. Chem. Phys. **152**, 194503 (2020).

[35] J. S. Langer, Shear-transformation-zone theory of plastic deformation near the glass transition, Phys. Rev. E **77**, 021502 (2008).

[36] J. S. Langer, Shear-transformation-zone theory of yielding in athermal amorphous materials, Phys. Rev. E **92**, 012318 (2015).

[37] P. Sollich, F. Lequeux, P. Hébraud, and M. E. Cates, Rheology of Soft Glassy Materials, Phys. Rev. Lett. **78**, 2020 (1997).

[38] P. Sollich, Rheological constitutive equation for a model of soft glassy materials, Phys. Rev. E **58**, 738 (1998).

[39] A. Nicolas, E. E. Ferrero, K. Martens, and J.-L. Barrat, Deformation and flow of amorphous solids: Insights from elastoplastic models, Rev. Mod. Phys. **90**, 045006 (2018).

[40] E. Lerner, E. DeGiuli, G. Düring, and M. Wyart, Breakdown of continuum elasticity in amorphous solids, Soft Matter **10**, 5085 (2014).

[41] E. Lerner, Mechanical properties of simple computer glasses, J. Non-Cryst. Solids **522**, 119570 (2019).

[42] A. Ninarello, L. Berthier, and D. Coslovich, Models and Algorithms for the Next Generation of Glass Transition Studies, Phys. Rev. X **7**, 021039 (2017).

[43] L. Berthier, D. Coslovich, A. Ninarello, and M. Ozawa, Equilibrium Sampling of Hard Spheres up to the Jamming Density and Beyond, Phys. Rev. Lett. **116**, 238002 (2016).

[44] R. Gutiérrez, S. Karmakar, Y. G. Pollack, and I. Procaccia, The static lengthscale characterizing the glass transition at lower temperatures, EPL (Europhys. Lett.) **111**, 56009 (2015).

[45] D. MacKay, macopt optimizer (2004), http://www.inference.org.uk/mackay/c/macopt.html.

[46] E. Lerner, G. Düring, and M. Wyart, Simulations of driven overdamped frictionless hard spheres, Comput. Phys. Commun. **184**, 628 (2013).

[47] E. Lerner, G. Düring, and M. Wyart, A unified framework for non-Brownian suspension flows and soft amorphous solids, Proc. Natl. Acad. Sci. USA **109**, 4798 (2012).

[48] T. C. Lubensky, C. L. Kane, X. Mao, A. Souslov, and K. Sun, Phonons and elasticity in critically coordinated lattices, Rep. Prog. Phys. **78**, 073901 (2015).

[49] E. Lerner, Quasilocalized states of self stress in packing-derived networks, Eur. Phys. J. E **41**, 93 (2018).

[50] L. D. Landau and E. M. Lifshitz, *Theory of Elasticity, Translated from the Russian by J. B. Sykes and W. H. Reid* (Pergamon London, 1959), p. 134.

[51] V. L. Gurevich, D. A. Parshin, and H. R. Schober, Anharmonicity, vibrational instability, and the boson peak in glasses, Phys. Rev. B **67**, 094203 (2003).

[52] D. A. Parshin, H. R. Schober, and V. L. Gurevich, Vibrational instability, two-level systems, and the boson peak in glasses, Phys. Rev. B **76**, 064206 (2007).

[53] C. Rainone, P. Urbani, F. Zamponi, E. Lerner, and E. Bouchbinder, Mean-field model of interacting quasilocalized excitations in glasses, SciPost Phys. Core **4**, 008 (2021).

[54] K. González-López, M. Shivam, Y. Zheng, M. P. Ciamarra, and E. Lerner, Mechanical disorder of sticky-sphere glasses. I. Effect of attractive interactions, Phys. Rev. E **103**, 022605 (2021).

[55] E. Bitzek, P. Koskinen, F. Gähler, M. Moseler, and P. Gumbsch, Structural Relaxation Made Simple, Phys. Rev. Lett. **97**, 170201 (2006).